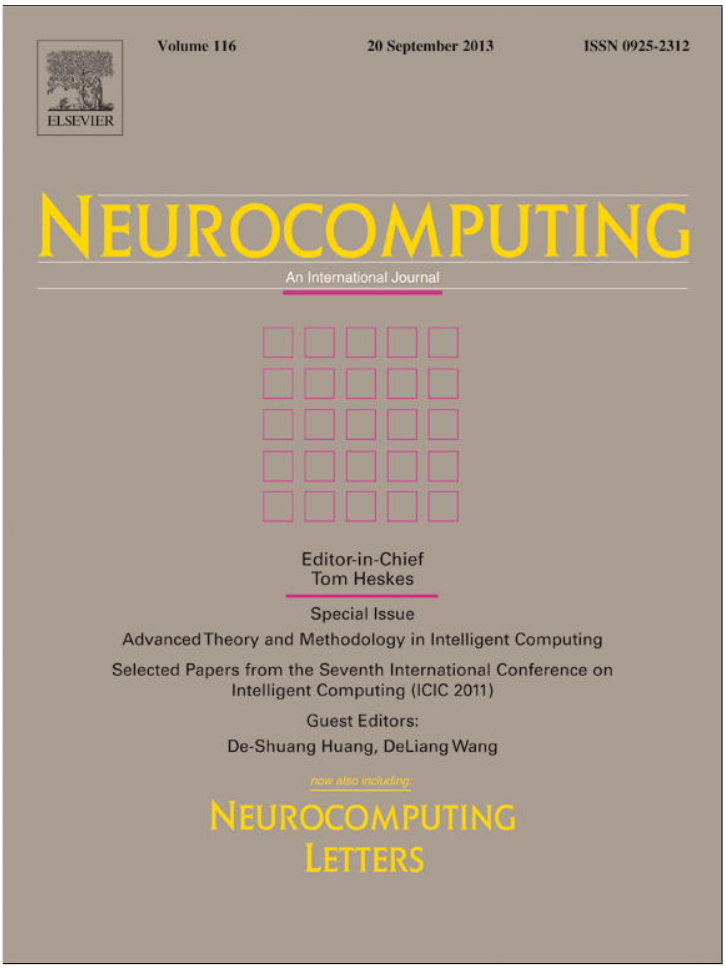

Neurocomputing 116 (2013) 157–164

Contents lists available at SciVerse ScienceDirect

Neurocomputing

journal homepage: www.elsevier.com/locate/neucom

Feature extraction through contourlet subband clustering for texture classification

Yongsheng Dong [a,b], Jinwen Ma [a,*]

[a] Department of Information Science, School of Mathematical Sciences and LMAM, Peking University, Beijing 100871, China
[b] Electronic Information Engineering College, Henan University of Science and Technology, Luoyang 471023, China

ARTICLE INFO

Available online 11 October 2012

Keywords:
Texture classification
Contourlet transform
Feature extraction
c-Means clustering

ABSTRACT

Feature extraction is an important processing procedure in texture classification. For feature extraction in the wavelet domain, the energies of subbands are usually extracted for texture classification. However, the energy of one subband is just a specific feature. In this paper, we propose an efficient feature extraction method for texture classification. In particular, feature vectors are obtained by *c*-means clustering on the contourlet domain as well as using two conventionally extracted features that represent the dispersion degree of contourlet subband coefficients. The *c*-means clustering algorithm is initialized via a nonrandom initialization scheme. By investigating these feature vectors, we employ a weighted L_1-distance for comparing any two feature vectors that represent the corresponding subbands of two images and define a new distance between two images. According to the new distance, a *k*-Nearest Neighbor (kNN) classifier is utilized to perform texture classification, and experimental results show that our proposed approach outperforms five current state-of-the-art texture classification approaches.

1. Introduction

Texture classification is one of the fundamental issues in computer vision and image processing. Various approaches for texture feature extraction as well as classification have been proposed during the last two decades [1–17], but the texture analysis and classification problem remains difficult and needs intensive research.

As a multiresolution analysis tool, the wavelet transform has been widely used for texture classification, which can be divided into model-based approaches and feature-based approaches. In the model-based approaches, the used models include the generalized Gaussian density (GGD) model [4], the bit-plane probability (BP) model [7], the refined histogram (RH) [8], the generalized gamma density (GΓD) model [9], and the like. These models are all under the assumption that wavelet subband coefficients follow some previously given parametric probability distributions. Texture classification is further performed by utilizing the parameters in the models which are estimated according to the subband coefficient. However, it can be found that for some texture images the parameters of the given parametric distribution of wavelet subband coefficients is difficult to be estimated. So, it is an alternative for us to utilize a nonparametric method to model or cluster the coefficients.

On the other hand, in feature-based approaches, the total energy of each high-pass wavelet subband is a commonly used statistical feature for texture classification [11]. Moreover, the local energy features in each high-pass subband can also be extracted and used to perform texture classification [12,13].

Recently, the contourlet transform was developed by Do and Vetterli [18] to get rid of the limitations of wavelets. Moreover, the contourlet expansion can achieve the optimal approximation rate for piecewise smooth functions with C^2 contours in some sense [18]. Therefore, it is valuable to utilize the contourlet transform to perform texture classification. Considering the advantage and disadvantage of the two kinds of wavelet-based methods, we attempt to combine nonparametric modeling with extracting features from the contourlet domain to perform texture classification.

As well-known, a typical nonparametric modeling method is to cluster the data in a given data set and represent them by the converged cluster centers. Among clustering algorithms [19–24], the *c*-means (or *k*-means) algorithm is a simple and popular clustering algorithm [19–21]. However, its performance heavily depends on the initial setting.

In this paper, by investigating the distribution of coefficients in each contourlet subband, we propose an efficient feature extraction approach for texture classification, which combines cluster features obtained by a *c*-means clustering algorithm using a nonrandom

* Corresponding author. Tel.: +86 10 62760609; fax: +86 10 62751801.
E-mail addresses: dongyongsheng93@163.com (Y. Dong), jwma@math.pku.edu.cn (J. Ma).

0925-2312/$ - see front matter © 2013 Elsevier B.V. All rights reserved.
http://dx.doi.org/10.1016/j.neucom.2011.12.059

initialization approach with conventional features extracted from contourlet subbands. In particular, we use a c-means clustering algorithm to cluster the contourlet coefficients, and the converged cluster centers are served as the features to represent the contourlet subband coefficients. Meanwhile, two conventional features representing the dispersion degree of contourlet subband coefficients are also extracted. In this way, a feature vector is formed for each contourlet subband by combining these two kinds of features together. Then, we employ the weighted L_1 metrics for measuring the feature vectors. Finally, we utilize a k-Nearest Neighbor (kNN) classifier based on the total distance obtained by summing up all the weighted L_1 metrics to perform the supervised texture classification, and experimental results on large texture datasets reveal that our proposed method outperforms five current state-of-the-art texture classification methods.

The rest of the paper is organized as follows. Section 2 introduces the contourlet transform. Section 3 presents the new texture classification method based on our proposed feature extraction approach. Experimental results are conducted in Section 4 to demonstrate the efficiency of our proposed feature extraction approach for texture classification. Finally, we conclude briefly in Section 5.

2. Contourlet transform

The primary goal of the contourlet construction was to obtain a sparse expansion for a typical image that is piecewise smooth [18]. Two-dimensional wavelets are only good at catching the point discontinuities, but do not capture the geometrical smoothness of the contours [25].

To get rid of the limitations of wavelets, the contourlet transform was constructed by utilizing a double filter bank structure in which at first the Laplacian pyramid is used to capture the point discontinuities, and then a directional filter bank (DFB) is used to link point discontinuities into linear structure [18]. Due to its cascade structure accomplished by combining the Laplacian pyramid with a DFB at each scale, multiscale and directional decomposition stages in the contourlet transform are independent of each other. Therefore, one can decompose each scale into any arbitrary power of two's number of directions, and different scales can be decomposed into different numbers of directions. Moreover, it can represent smooth edges with close to optimal efficiency. More recent developments and applications on the contourlet transform can be found in [25–27].

Fig. 1 shows an example of the contourlet transform on the "Lena" image. For the visual clarity, only two-scale decompositions are shown. The image is decomposed into a lowpass subband and 16 bandpass directional subbands with 8 subbands at each scale.

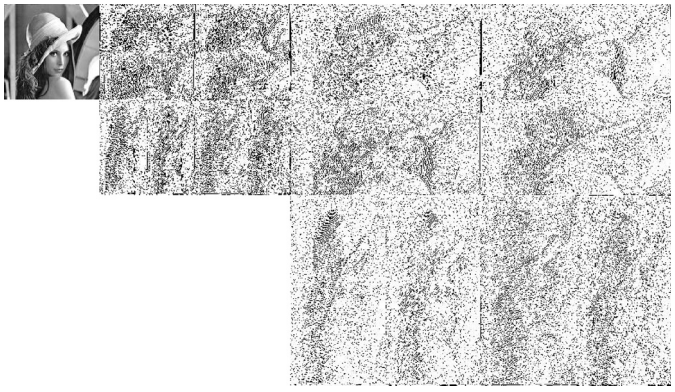

Fig. 1. Contourlet transform of the "Lena" image. The image is decomposed into a lowpass subband and 16 bandpass directional subbands with eight subbands at each scale. Small coefficients are colored black while large coefficients are colored white.

3. New texture classification method

For a texture image, denoted by a matrix $\mathbf{a}_0$, we can decompose it via the discrete contourlet transform into a set of coefficients, which are also denoted by matrixes $\{\mathbf{a}_L, \mathbf{c}_{i,j}^{(l_i)}\}$, $i=1,2,\ldots,L$ and $j=1,\ldots,2^{l_i}$. Note that the indexes i and j specify the scale and direction, respectively. L is the number of scales, while the number of DFB decomposition levels varies with the scale i, being denoted by l_i. For simplicity, we set the number of DFB decomposition levels at each scale as 3 ($l_i=3$, $i=1,2,\ldots,L$), that is, the number of directional subbands at each scale is 8.

For L-scale contourlet decompositions of a given texture image, the average amplitude of the coefficients increases almost exponentially with the scale i ($i=1,2\ldots,L$). So, to uniformly measure the contourlet coefficients at different scales, we regularize them by multiplying the factor $1/4^i$ to those in the high-pass directional subbands at the i-th scale, and multiplying the factor $1/4^L$ to those in the low-pass subband. For the sake of clarity, the contourlet coefficients in the following will represent the regularized coefficients without explanation.

3.1. Proposed feature extraction method

Feature extraction is very important for the purpose of pattern recognition such as texture classification [11–14], handwritten numeral recognition [25], face recognition [28–31], and so on. In this subsection, some important features are extracted from contourlet subbands for texture classification.

3.1.1. Features extracted by c-means clustering

Consider a particular contourlet subband with N coefficients $S=\{x_1,x_2,\ldots,x_N\}$. As an important approach in data mining, clustering analysis has its advantage in mining valuable information from a number of data. Actually, many statistical methods need to model the data by a previously assumed parametric distribution. However, clustering analysis does not need any parametric assumption. In this paper, we attempt to mine the essential information by employing a clustering algorithm and define some features representing the contourlet subband for classification. Various algorithms have been established to solve the clustering problem [19–24]. Among them, the c-means algorithm is a simple and popular one. Its idea is to partition this data set into J disjoint subsets (clusters) $C_1,\ldots,C_J$ such that a clustering error criterion is optimized [20]. The criterion is the sum of the squared Euclidean distances between each data point x_i and the centroid f_j (cluster center) of the subset C_j which contains x_i, which is called clustering error and given by

$$E(f_1,\ldots,f_J)=\sum_{i=1}^{N}\sum_{j=1}^{J} I_{C_j}(x_i)\|x_i-f_j\|^2, \tag{1}$$

where $I_C(x)=1$ if $x\in C$ and 0 otherwise.

However, the c-means clustering algorithm suffers from the serious drawback that its performance heavily depends on the initial setting [19]. For the purpose of clustering on the contourlet subband with N coefficients, we let $\delta=[N/2J]$, where $[z]$ denotes the largest integer less than or equal to z. In this way, we divide the N coefficients into J subsets:

$$[\tilde{x}_1,\tilde{x}_{2\delta+1}),[\tilde{x}_{2\delta+1},\tilde{x}_{4\delta+1}),\ldots,[\tilde{x}_{2(J-1)\delta+1},\tilde{x}_N)], \tag{2}$$

where $\tilde{x}_i$ denotes the i-th order statistic of the coefficient sample $S=\{x_1,x_2,\ldots,x_N\}$. Moreover, the centers of these subsets, f_j,

$j=1,2,\ldots,J$, can be denoted approximately by

$$f_j=\tilde{x}_{t_j}, \tag{3}$$

where $t_j=(2j-1)*\delta$. In this way, we can initialize the cluster center f_j using Eq. (3), $j=1,2,\ldots,J$. Note that the initial values obtained by this scheme are determinative and unique, which can be seen clearly according to the definition of order statistic. The main reason that we adopt this initialization scheme rather than a random initialization scheme is to avoid the fluctuation and uncertainty of clustering and classification performance caused by the randomness of initial starting condition. Moreover, it has been verified by our experimental results that our proposed initialization scheme performs better than or as well as the random initialization scheme when they are used in the c-means clustering and further texture classification.

It is important to note that the converged cluster centers $f_1,\ldots,f_J$ are real numbers. We sort and denote them still by $f_1,\ldots,f_J$ for convenience. Obviously, the vector

$$F^1=(f_1,\ldots,f_J) \tag{4}$$

can be used as the features to represent the contourlet subband coefficients. Fig. 2 shows two textures "Leaves.0003" and "Leaves.0012" obtained from [32], which are very homogeneous. After having implemented the 4-level contourlet transform with eight directional subbands at each scale, we can extract features from each of the 33 resulting contourlet subbands with the above c-means clustering algorithm. Fig. 3 plots the histograms of coefficients in the j-th directional subbands $\mathbf{c}_{i,j}$ and $\mathbf{c}'_{i,j}$ at the i-th scale corresponding to the two texture images, respectively, where $i=4$ and $j=1$.

Generally speaking, Gaussian mixture model (GMM) [33–38] can be used to model the samples whose distribution is unknown. However, for the contourlet subband coefficients corresponding to these two images, the usually used learning algorithms [33–38] for Gaussian mixtures do not converge well in such complicated cases. To get rid of this difficulty, we here adopt the c-means clustering algorithm to extract features. In fact, the learning algorithm for GMM makes a soft assignment based on the posterior probabilities. However, the c-means algorithm performs a hard assignment of data points to clusters, in which each data point is associated uniquely with one cluster. So we adopt the c-means algorithm to cluster the contourlet subband coefficients. The clustered feature values of the two texture images are shown in the horizontal axises of Fig. 3(a) and (b), respectively. As seen from Fig. 3, although the two images are very homogeneous and confusing, the clustered features of them are different. So, the clustered features we extract by clustering have good discrimination in recognizing texture images.

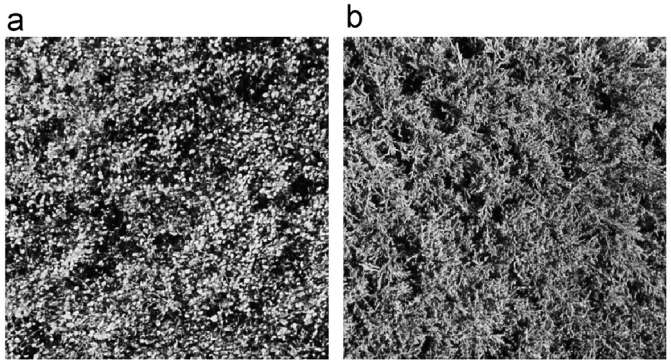

Fig. 2. The textures "Leaves.0003" and "Leaves.0012".

3.1.2. Conventional features

As the clustered features may not suffice for texture classification, certain important conventional features can be added. For the clustered features extracted by c-means clustering, the obvious extension is the measurement of the dispersion degree of subband coefficients, which is equivalent to the dispersion degree of the cluster centers in some sense. In fact, the clustered features are the first-order ones. From a statistical point of view, the second-order statistics, (sample) variance and second-order origin (sample) moment (Norm-2 energy), can represent the dispersion degree of sample. So we utilize these two statistics to measure the dispersion degree of subband coefficients, which are defined as

Variance:

$$f_{J+1}=\frac{1}{N}\sum_{n=1}^{N}(x_n-\overline{x}_N)^2, \tag{5}$$

where

$$\overline{x}_N=\frac{1}{N}\sum_{i=1}^{N}x_n$$

and

Norm-2 energy:

$$f_{J+2}=\frac{1}{N}\sum_{n=1}^{N}x_n^2, \tag{6}$$

respectively. So, we can obtain the feature vector F for the contourlet subband, which is given by

$$F=(f_1,\ldots,f_J,f_{J+1},f_{J+2}). \tag{7}$$

The workflow chart for our proposed feature extraction method is shown in Fig. 4. Next we shall give the discrepancy measurement between any two feature vectors.

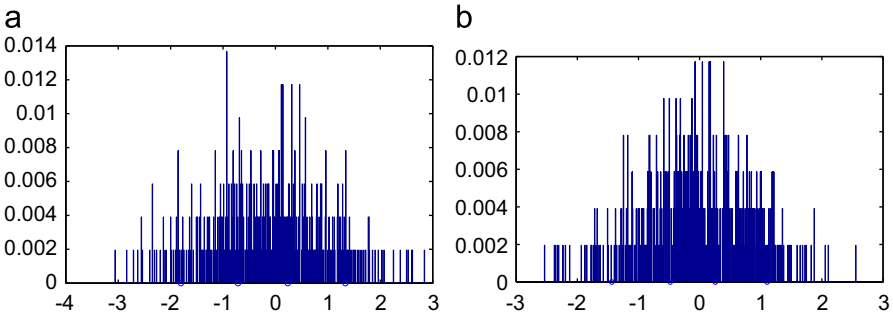

Fig. 3. The histograms of the textures "Leaves.0003" and "Leaves.0012". The little circles in the horizontal axises of the two coordinate systems represents the clustered features of the two texture images obtained by the c-means clustering algorithm.

3.2. Discrepancy measurement of feature vectors

Once the feature vectors of all subbands are obtained for every texture, we can compare the corresponding feature vectors of two subbands using a discrepancy metric. According to the characterization of the feature vectors, we use the Relative-L1 (abbreviated as RL1) distance as the discrepancy metric of two feature vectors F^1 and F^2, which is given by

$$RL_1(F^1,F^2)=\sum_{j=1}^{\tau}\frac{|f_j^1-f_j^2|}{1+|f_j^1|+|f_j^2|}, \tag{8}$$

where $F^1=(f_1^1,\ldots,f_\tau^1)$, $F^2=(f_1^2,\ldots,f_\tau^2)$ and $\tau=J+2$. Note that the RL1 distance is a weighted L_1 one.

Given two images I_1 and I_2, to measure the distance between them, we first perform an L-scale contourlet transform on each of them and obtain M contourlet subbands for each image. For clarity, they are denoted as $(B_1^{I_1},B_2^{I_1},\ldots,B_M^{I_1})$ and $(B_1^{I_2},B_2^{I_2},\ldots,B_M^{I_2})$, respectively, where $M=8L+1$ Then, the distance between the two images is defined as the total distance (TD) of all the corresponding RL_1 ones, which is given by

$$TD(I_1,I_2)=\sum_{t=1}^{M}d_t, \tag{9}$$

where $d_t=RL_1(F_t^1,F_t^2)$ is the RL1 distance between the two feature vectors F_t^1 and F_t^2 corresponding to the subbands $B_t^{I_1}$ and $B_t^{I_2}$, respectively, for $t=1,2,\ldots,M$.

3.3. Classification

Given a test texture patch P and a training texture patch sample set, we utilize a k-nearest-neighbor (kNN) classifier to perform supervised texture classification. The kNN classifier assign P to the class to which the majority of these k nearest neighbors belong.

In particular, we first perform a L-scale contourlet transform to an unknown (test) texture patch and all the training texture patches, and then extract the features from all the contourlet subbands of each patch. Finally, we compute the distances between the test patch and each training texture patch according to the above TD distance and utilize the k-nearest-neighbor classifier to perform texture classification. Table 1 summarizes the procedure of our proposed supervised texture classification method.

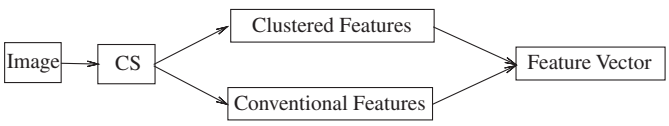

Fig. 4. The workflow chart of the proposed feature extraction method, where CS denotes contourlet subbands, clustered features refer to $F^1=(f_1,\ldots f_J)$, conventional features refer to f_{J+1} and f_{J+2}, and feature vector refers to $F=(f_1,\ldots f_J f_{J+1} f_{J+2})$.

4. Experimental results

In this section, various experiments are carried out to demonstrate our proposed feature extraction method for texture classification. In our experiments, we select the pyramid and directional filters by the "9–7" filters in the contourlet transform, which are the biorthogonal wavelet filters. For the sake of clarity, we refer to our proposed method based on Contourlet Subband Clustering and the TD distance as CSC+TD.

4.1. Classification performance

We first evaluate CSC+TD on the texture set that consists of 32 grey 640×640 images (denoted by Set-1) from the Brodatz database [39], which is also used in [16]. In this experiment, each image is divided into 16 160×160 nonoverlapping patches. Eight training samples are selected from each of 32 classes and let the other samples for test, that is, the training sample set is separated from the test sample set. The average classification accuracy rate (ACAR) is computed over the experimental results on 10 random splits of the training and test sets.

As for the number k in the kNN classifier of CSC+TD, we simply set it as 1. In fact, we have considered the other possible values of the k. However, the experimental results reveal that the optimal classification performance is always obtained at $k=1$. For example, Fig. 5 shows the classification performance of CSC+TD on Set-1 with respect to the number of training samples for the different values of k in the kNN classifier in the case of $L=4$ and $J=3$. It is clear that the kNN classifier with $k=1$ outperforms $k=3$ and $k=5$. So we utilize $k=1$, that is, one-nearest-neighbor classifier, in our experiments.

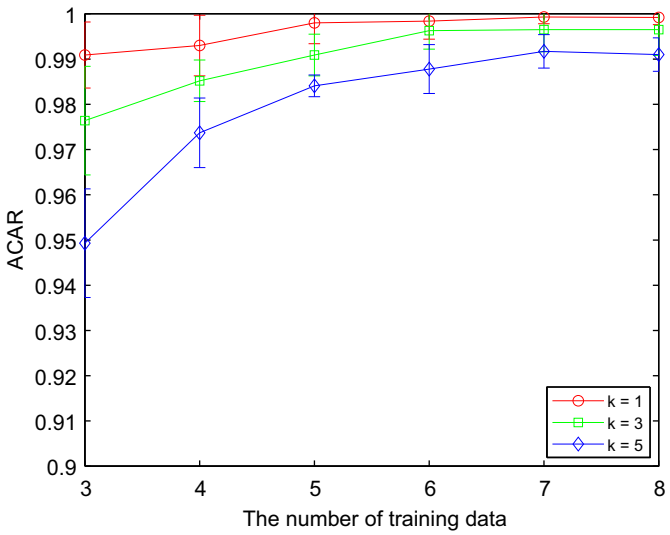

Fig. 5. The classification performance of our proposed CSC+TD with respect to the number of training samples for the different values of k in the kNN classifier in the case of $L=4$ and $J=3$.

Table 1
The procedure of our proposed supervised texture classification method.

[Input:] Training texture patches selected from each texture image or class, and a test texture patch
[Output:] The label of the test texture patch
(1) Decompose a patch of a given texture image or class with the L-scale contourlet transform into M contourlet subbands
(2) Compute the feature vectors (7) of each contourlet subband according to Eqs. (4)–(6)
(3) Repeat the above two steps for all the training patches of all the texture classes and the test texture patch, and obtain the feature vectors for them
(4) Compute all the distances of the test texture image to all training texture patches by use of the total distance TD of two images
(5) Assign the test texture image to the class to which the majority of the k nearest neighbors belong

To investigate the sensitivity of the cluster number J to classification performance, Fig. 6(a)–(e) summarize the classification performance of CSC+TD on Set-1 with J being 1,2 ...,5 when the number of the decomposition scales is 1,2 ...,5, respectively. As seen from them, the ACAR of CSC+TD with each value of J increases monotonically with the number of training samples for each value of L. The ACAR of CSC+TD with $J=3$ is highest among those of CSC+TD with the five values of J for $L=1,2,\ldots,4$ although it is not evident for $L=5$. Certainly, it is also observed that the ACARs of CSC+TD ($J=4$) and CSC+TD ($J=5$) are only slightly less than that of CSC+TD ($J=3$), especially for $L=3,\ldots,5$. For the statistical viewpoint, it seems that we should select the cluster number J from the three numbers (3–5). However, for the pattern recognition purpose, we should select the recognition approach that extracts the less number of feature vectors whose dimension is smaller if two approaches have the almost same recognition performance. In our proposed method, the smaller the cluster number, the smaller the dimension of the feature vector for each contourlet subband we utilize for texture classification. So the optimal selection of J is $J=3$.

The classification performance of CSC+TD ($J=3$) with $L=1,2,\ldots,5$ are summarized in Fig. 7. It is clear that CSC+TD ($L=4,J=3$) and CSC+TD ($L=5,J=3$) almost have the same classification performance, and both of them outperform CSC+TD ($J=3$) with the smaller number of the contourlet decomposition scales. Due to that the number of feature vectors for $L=4$ is less than for $L=5$, we consider that the optimal selection of L should be $L=4$. As seen from Fig. 7, the ACAR of CSC+TD with the optimal parameter values ($k=1$, $J=3$, $L=4$) is 99.92%, which shows the efficiency of our proposed CSC+TD. Further comparisons with other methods will be given in the next subsection, and these optimal values of the three parameters will also be used in the following experiments.

4.2. Comparisons with other methods

We further compare CSC+TD with the other current state-of-the-art methods of texture classification on different texture image sets. Actually, three additional texture image sets are used, denoted by Set-2, Set-3, Set-4, respectively. Set-2 consists of 80 grey 640×640 images (shown in Fig. 8) from the Brodatz database [39], which was also used in [16]. Set-3 consists of 30 texture images of size 512×512 (shown in Fig. 9), which were used in [14] and can be downloaded from the VisTex database [32]. Set-4 consists of 50 VisTex texture images (shown in Fig. 10). In the experiments on Set-2, each image is divided into sixteen 160×160 nonoverlapping patches, and thus there are totally 1280 samples available. For both Set-3 and Set-4, each image is divided into 16 128×128 nonoverlapping patches, and thus there are totally 480 and 800 samples available, respectively. For the purpose of supervised classification on each of these three texture image datasets, we select eight training patches from each of the texture classes and let the other patches for test.

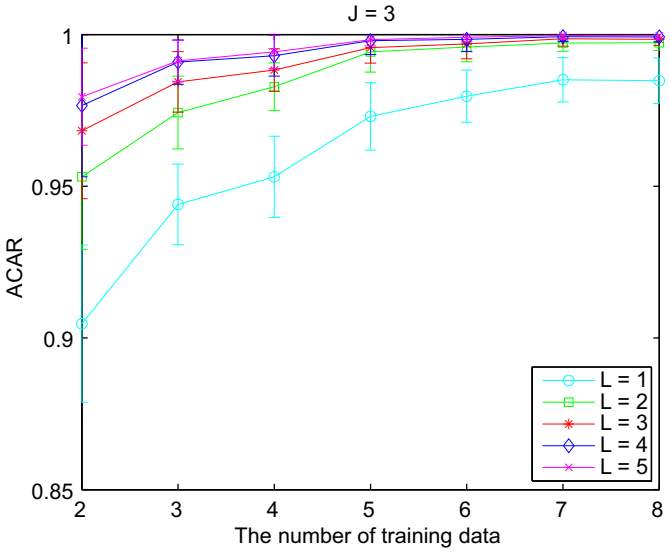

Fig. 7. The classification performance of our proposed CSC+TD with respect to the number of training samples when the cluster number J is 3.

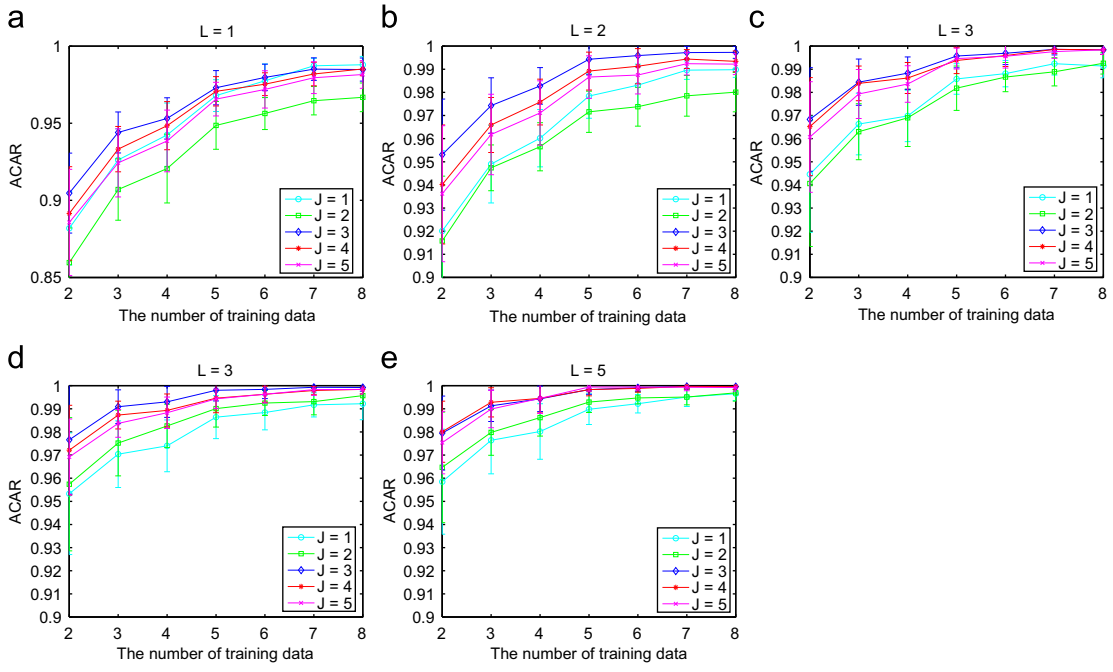

Fig. 6. The classification performance of our proposed CSC+TD with respect to the number of training samples for the different numbers of the contourlet decomposition scale: (a) $L=1$; (b) $L=2$; (c) $L=3$; (d) $L=4$; (e) $L=5$.

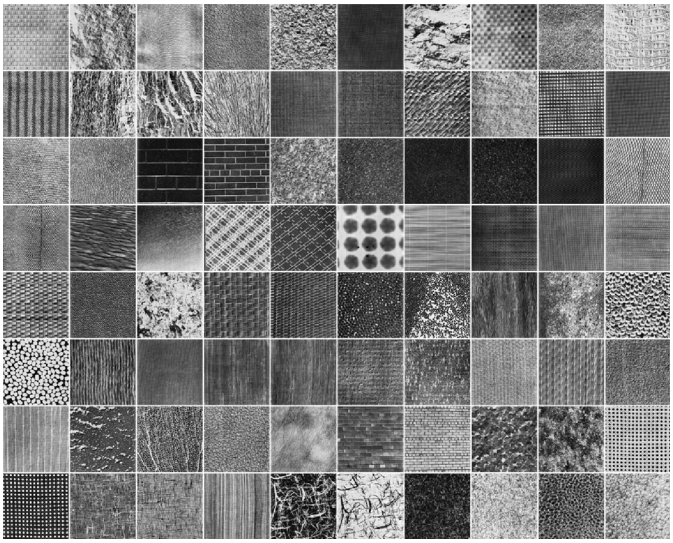

Fig. 8. 80 Brodatz texture images in Set-2.

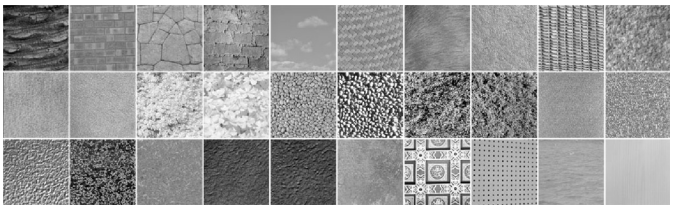

Fig. 9. 30 VisTex texture images in Set-3.

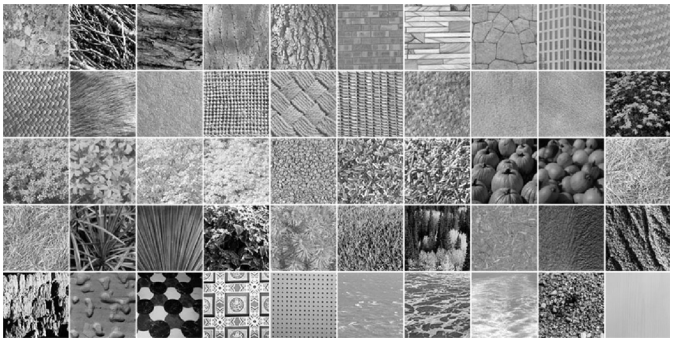

Fig. 10. 50 VisTex texture images in Set-4.

To demonstrate the efficiency of our proposed CSC+TD, we compare it with three current state-of-the-art methods of texture classification. The first is the method based on the singular value decomposition (SVD) and the Kullback–Leibler distance (KLD) (referred to as SVD+KLD) [12]. The second one is the method based on the bit-plane probability (BP) signature and the minimum distance (MD) classifier(referred to as BP+MD) [7]. The third method is based on the local binary pattern (LBP) (referred to as LBP), which was proposed in [15].

Table 2 reports the classification results of these methods. As seen from it, for the classification experiments on Set-2, CSC+TD performs better than these three methods by at least 2.06%. To provide additional justification of our proposed method, we compare CSC+TD with the texture classification method based on the local pattern and Gaussian mixture model (referred to as LP+GMM) in [16]. CSC+TD outperforms LP+GMM by 3.37%. On Set-3, CSC+TD performs better than these three methods by at least 2.12%, and outperforms the ridgelet method [14] by 2.46%. Moreover, CSC+TD performs better than these three methods by at least 2.38% on the larger VisTex texture dataset Set-4.

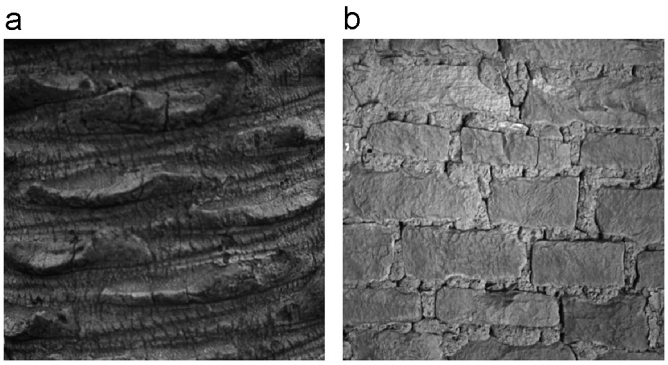

Fig. 11. Two textures of Set-3 that cannot be recognized without error by our proposed CSC+TD. From left to right: (a) Bark.0006 and (b) Brick.0005.

Table 2
The average classification accuracy rates (%) of the six methods on the three datasets.

Methods	Set-2	Set-3	Set-4
LP+GMM [16]	93.44	n.a.	n.a.
Ridgelet method [14]	n.a.	96.79	n.a.
SVD+KLD [12]	49.22 ± 1.85	41.17 ± 3.31	36.35 ± 2.14
BP+MD [7]	88.16 ± 1.03	96.79 ± 0.62	79.53 ± 1.26
LBP [15]	94.75 ± 1.02	97.13 ± 0.80	83.57 ± 1.09
CSC+TD	96.81 ± 0.44	99.25 ± 0.38	85.95 ± 1.50

To compare intensively with the three methods (SVD+KLD, BP+MD, LBP), the classification accuracy rates of all 30 texture classes in Set-3 are computed and shown in Table 3. It can be observed that our method performs better than or as well as the other three methods for 28 texture classes. CSC+TD arrive 100% classification accuracy rate on these 28 texture classes, which is larger than the number of the texture classes recognized with no error by LBP, 18, and clearly exceeds those by the other methods. There are only two texture classes that cannot be recognized without error. They are given in Fig. 11. This shows the superiority of contourlet in capturing directional information. As far as the ACAR for the whole dataset, the mean of the ACARs for all classes, is concerned, our proposed CSC+TD outperforms the three methods by 2.12%–58.08%.

4.3. Discussions on computational cost

All the experiments in this paper have been implemented on a workstation with Intel(R) Core(TM) i5 CPU (3.2 GHz) and 3G RAM in Matlab environment. The number of training samples used in the experiments is 8. Table 4 reports the time used for texture classification for the four methods (CSC+TD, LBP, BP+MD, and SVD+KLD). As seen from Table 4, the time for texture classification (TTC) of CSC+TD for the 30 texture dataset is 80.27s, which is less than the TTC of LBP and BP+MD, especially BP+MD. Although SVD+KLD is faster than our method, the ACAR of SVD+KLD is only 41.17%. In the CSC+TD method, the most costly part is the clustering process. Our proposed CSC+TD method will be more faster if a more efficient clustering algorithm can be used in the clustering process.

In summary, our proposed CSC+TD performs better than five current state-of-the-art texture classification methods (LP+GMM, Ridgelet Method, SVD+KLD, BP+MD, and LBP) on the classification

Table 3
The average classification accuracy rate (%) for each of 30 texture classes in Set-3 with the four methods: Column 1: CSC+TD, Column 2: LBP, Column 3: BP+MD, Column 4: SVD+KLD.

	1	2	3	4		1	2	3	4
Bark.0006	82.50	85.00	61.25	3.75	Food.0001	100	100	100	100
Brick.0000	100	100	100	22.50	Leaves.0003	100	100	100	25.00
Brick.0004	100	92.50	100	13.75	Leaves.0012	100	100	100	25.00
Brick.0005	95.00	100	88.75	21.25	Metal.0000	100	100	93.75	47.50
Clouds.0001	100	78.75	100	48.75	Metal.0002	100	100	100	43.75
Fabric.0000	100	95.00	95.00	96.25	Metal.0004	100	100	100	50.00
Fabric.0006	100	92.50	88.75	36.25	Misc.0001	100	98.75	100	11.25
Fabric.0007	100	100	90.00	50.00	Misc.0002	100	100	100	21.25
Fabric.0013	100	100	100	88.75	Sand.0000	100	90.00	100	28.75
Fabric.0015	100	100	100	53.75	Sand.0002	100	97.50	100	33.75
Fabric.0017	100	100	100	57.50	Stone.0005	100	91.25	100	27.50
Fabric.0019	100	100	100	47.50	Tile.0004	100	100	100	52.50
Flowers.0005	100	96.25	96.25	60.00	Tile.0008	100	100	98.75	26.25
Flowers.0006	100	98.75	100	26.25	Water.0005	100	97.50	100	52.50
Food.0000	100	100	100	38.75	Wood.0002	100	100	91.25	25.00
					Mean	99.25	97.13	96.79	41.17

Table 4
The time for texture classification (TTC) (in seconds) using the four methods on Set-3.

CSC+TD	LBP	BP+MD	SVD+KLD
80.27	126.79	207.83	17.02

accuracy rate. The main reason is that CSC+TD utilizes the contourlet transform to decompose texture images and efficiently extracts the feature vectors representing the distribution characterizations of contourlet subband coefficients. As with the TTC, SVD+KLD is the more efficient than CSC+TD, but its ACAR is unsatisfactory. If we take into account the TTC and ACAR, the results clearly show that our proposed CSC+TD outperforms other methods.

5. Conclusions

In this paper, we have investigated the texture classification problem and established a novel texture classification method via nonparametric modeling through *c*-means clustering on the contourlet domain as well as extracting two conventional features that represent the dispersion degree of coefficients from contourlet subbands. According to the weighted L1-distance between feature vectors, a new distance between two images is defined, with which a *k*-nearest neighbor classifier is utilized to perform supervised texture classification. The various experiments have shown that our proposed method significantly improves the texture classification accuracy in comparison with five current state-of-the-art texture classification methods.

Acknowledgments

This work was supported by the Natural Science Foundation of China for Grant 60771061. A preliminary version of this work was presented at the 2011 Seventh International Conference on Intelligent Computing (ICIC 2011), August 11–14, 2011, Zhengzhou, China, LNAI, vol. 6839, pp. 421–426. The authors would like to thank Dr. S.K. Choy and Prof. C.S. Tong, Hong Kong Baptist University, for providing the source code of the bit-plane probability (BP) based method (BP+MD).

References

[1] A. Laine, J. Fan, Texture classification by wavelet packet signatures, IEEE Trans. Pattern Anal. Mach. Intell. 15 (11) (1993) 1186–1191.
[2] T. Randen, J.H. Husoy, Filtering for texture classification: a comparative study, IEEE Trans. Pattern Anal. Mach. Intell. 21 (4) (1999) 291–310.
[3] M. Unser, Texture classification and segmentation using wavelet frames, IEEE Trans. Image Process. 4 (11) (1995) 1549–1560.
[4] M.N. Do, M. Vetterli, Wavelet-based texture retrieval using generalized gaussian density and Kullback–Leibler distance, IEEE Trans. Image Process. 11 (2) (2002) 146–158.
[5] X. Liu, D.L. Wang, Texture classification using spectral histograms, IEEE Trans. Image Process. 12 (6) (2003) 661–670.
[6] S.K. Choy, C.S. Tong, Supervised texture classification using characteristic generalized Gaussian density, J. Math. Imaging Vision 29 (1) (2007) 35–47.
[7] S.K. Choy, C.S. Tong, Statistical properties of bit-plane probability model and its application in supervised texture classification, IEEE Trans. Image Process. 17 (8) (2008) 1399–1405.
[8] L. Li, C.S. Tong, S.K. Choy, Texture classification using refined histogram, IEEE Trans. Image Process. 19 (5) (2010) 1371–1378.
[9] S.K. Choy, C.S. Tong, Statistical wavelet subband characterization based on generalized Gamma density and its application in texture retrieval, IEEE Trans. Image Process. 19 (2) (2010) 281–289.
[10] G.V.D. Wouwer, P. Scheunders, D.V. Dyck, Statistical texture characterization from discrete wavelet representations, IEEE Trans. Image Process. 8 (4) (1999) 592–598.
[11] S.C. Kim, T.J. Kang, Texture classification and segmentation using wavelet packet frame and Gaussian mixture model, Pattern Recognition 40 (4) (2007) 1207–1221.
[12] S. Selvan, S. Ramakrishnan, SVD-based modeling for image texture classification using wavelet transformation, IEEE Trans. Image Process. 16 (11) (2007) 2688–2696.
[13] Y. Dong, J. Ma, Wavelet-based image texture classification using local energy histograms, IEEE Signal Process. Lett. 18 (4) (2011) 247–250.
[14] S. Arivazhagan, L. Ganesan, T.G. Subash Kumar, Texture classification using ridgelet transform, Pattern Recognition Lett. 27 (16) (2006) 1875–1883.
[15] T. Ojala, M. Pietikainen, T.T. Maenpaa, Multiresolution gray-scale and rotation invariant texture classification with local binary pattern, IEEE Trans. Pattern Anal. Mach. Intell. 24 (7) (2002) 971–987.
[16] H. Lategahn, S. Gross, T. Stehle, T. Aach, Texture classification by modeling joint distributions of local patterns with Gaussian mixtures, IEEE Trans. Image Process. 19 (6) (2010) 1548–1557.
[17] Z.H. Guo, L. Zhang, D. Zhang, A completed modeling of local binary pattern operator for texture classification, IEEE Trans. Image Process. 19 (6) (2010) 1657–1663.
[18] M.N. Do, M. Vetterli, The contourlet transform: an efficient directional multiresolution image representation, IEEE Trans. Image Process. 14 (12) (2005) 2091–2106.
[19] J.A. Lozano, J.M. Pena, P. Larranaga, An empirical comparison of four initialization methods for the k-means algorithm, Pattern Recognition Lett. 20 (1999) 1027–1040.
[20] A. Likas, M. Vlassis, J. Verbeek, The global k-means clustering algorithm, Pattern Recognition 36 (2) (2003) 451–461.
[21] A.M. Bagirov, Modified global k-means algorithm for sum-of-squares clustering problem, Pattern Recognition 41 (10) (2008) 3192–3199.
[22] G. Govaert, M. Nadif, Clustering with block mixture models, Pattern Recognition 36 (2) (2003) 463–473.
[23] J. Ma, T. Wang, A cost-function approach to rival penalized competitive learning (RPCL), IEEE Trans. Syst. Man Cybern. Part—B: Cybern. 36 (4) (2006) 722–737.

[24] S.Z. Selim, K.S. Al-Sultan, A simulated annealing algorithm for the clustering, Pattern Recognition 24 (10) (1991) 1003–1008.
[25] D.D.-Y. Po, M.N. Do, Directional multiscale modeling of images using the contourlet transform, IEEE Trans. Image Process. 15 (6) (2006) 1610–1620.
[26] G.Y. Che, B. Kegl, Invariant pattern recognition using contourlets and AdaBoost, Pattern Recognition 43 (3) (2010) 579–583.
[27] R. Eslami, H. Radha, Translation-invariant contourlet transform and its application to image denoising, IEEE Trans. Image Process. 15 (11) (2006) 3362–3374.
[28] Z.-Q. Zhao, D.S. Huang, B.-Y. Sun, Human face recognition based on multiple features using neural networks committee, Pattern Recognition Lett. 25 (12) (2004) 1351–1358.
[29] Z.-Q. Zhao, D.S. Huang, B.-Y. Sun, Human facial recognition based on multiple feature domains, in: The 5th World Congress on Intelligent Control and Automation (WCICA04), Hangzhou, China, June 14–18, 2004, pp. 4150–4155.
[30] W.S. Chen, P.C. Yuen, J. Huang, D.Q. Dai, Kernel machine-based one-parameter regularized fisher discriminant method for face recognition, IEEE Trans. Syst. Man Cybern. 35 (4) (2005) 659–669.
[31] L. Guo, D.S. Huang, Human face recognition based on Radial basis probabilistic neural network, in: International Joint Conference on Neural Networks (IJCNN2003), Portland, Oregon, July 20–24, 2003, pp. 2208–2211.
[32] 〈http://vismod.media.mit.edu/vismod/imagery/VisionTexture/vistex.html〉.
[33] R.A. Render, H.F. Walker, Mixture densities, maximum likelihood and the EM algorithm, SIAM Rev. 26 (2) (1984) 195–239.
[34] P. Guo, C.L.P. Chen, M.R. Lyu, Cluster number selection for a small set of samples using the Bayesian Ying-Yang model, IEEE Trans. Neural Networks 13 (3) (2002) 757–763.
[35] J.J. Verbeek, N. Vlassis, B. Krose, Efficient greedy learning of Gaussian mixture models, Neural Comput. 15 (2) (2003) 469–485.
[36] J. Ma, T. Wang, L. Xu, A gradient BYY harmony learning rule on Gaussian mixture with automated model selection, Neurocomputing 56 (2004) 481–487.
[37] J. Ma, X. He, A fast fixed-point BYY harmony learning algorithm on Gaussian mixture with automated model selection, Pattern Recognition Lett. 29 (6) (2008) 701–711.
[38] J. Ma, J. Liu, The BYY annealing learning algorithm for Gaussian mixture with automated model selection, Pattern Recognition 40 (7) (2007) 2029–2037.
[39] 〈http://www.ux.uis.no/tranden/brodatz.html〉.

Yongsheng Dong received the M.S. degree in applied mathematics from Wuhan University in 2005 and the Ph.D. degree in applied mathematics from Peking University in 2012. He is now with the Electronic Information Engineering College, Henan University of Science and Technology, Luoyang, China. His current research interests include image processing, pattern recognition, wavelets, and statistical machine learning.

Jinwen Ma received the M.S. degree in applied mathematics from Xi'an Jiaotong University in 1988 and the Ph.D. degree in probability theory and statistics from Nankai University in 1992. From July 1992 to November 1999, he was a lecturer or associate professor at Department of Mathematics, Shantou University. From December 1999, he became a full professor at Institute of Mathematic, Shantou University. From September 2001, he has joined the Department of Information Science at the School of Mathematical Sciences, Peking University, where he is currently a full professor and Ph.D. tutor. During 1995 and 2003, he also visited several times at the Department of Computer Science and Engineering, the Chinese University of Hong Kong as a research associate or fellow. He also worked as Research Scientist at Amari Research Unit, RIKEN Brain Science Institute, Japan from September 2005 to August 2006. He has published over 100 academic papers on neural networks, pattern recognition, bioinformatics, and information theory.